PHYSICS OF PLASMAS **23**, 092113 (2016)

Fast, hot electron production and ion acceleration in a helicon inductive plasma

Yung-Ta Sung,[a),b)] Yan Li,[a)] and John E. Scharer
Department of Electrical and Computer Engineering, University of Wisconsin-Madison, 1415 Engineering Drive, Madison, Wisconsin 53706, USA

(Received 14 June 2016; accepted 30 August 2016; published online 23 September 2016)

A large, time-averaged, double layer-like plasma potential drop of 80 V over several hundred Debye lengths has been observed in the magnetic expansion region on the Madison Helicon eXperiment. It is operated in an inductive mode at 900 W and low argon operating pressures (0.12–0.20 mTorr) in the collisionless regime. The plasma space potential drop is due to the formation of a double layer-like structure in the magnetic expansion region and is much higher than the potential drop caused by a Boltzmann expansion. With the plasma potential drop, a locally negative potential ion hole region at lower pressures with a higher electron density than ion density has been observed just the downstream of the potential drop region. Two-temperature Maxwellian electron distributions with a warm ($T_e \approx 15$ eV) and bulk ($T_e \approx 5$ eV) components are observed just upstream of the double layer validated through a RF compensated Langmuir probe and an optical emission spectroscopy (OES) diagnostics. In the expansion chamber downstream of the double layer-like potential drop, a single warm ($T_e \approx 15$ eV) Maxwellian electron distribution is observed via both the Langmuir probe and OES diagnostics. Ion beam energies of 65 eV are also observed downstream of the potential drop. *Published by AIP Publishing.*
[http://dx.doi.org/10.1063/1.4962758]

I. INTRODUCTION

Helicon plasmas have produced[1–5] double layers in the magnetic expansion plasmas that yield ion acceleration and electron temperatures that are different in the upstream and downstream regions. We have previously[2,3] examined double layer effects including plasma self bias that occur in a lower density (10^{8-9} cm^{-3}), capacitive coupling helicon regime. We recently examined[1] inductively coupled, moderate density (10^{10-11} cm^{-3}) helicon plasmas that exhibit a higher ($T_e = 13$ eV) electron temperature downstream of the double layer and a lower (4 eV) electron temperature upstream of the double layer by means of a Langmuir probe with a slight rise in the plasma potential downstream of the double layer.

In this paper, we utilize an additional diagnostics including a two-Maxwellian electron temperature optical emission spectra (OES) analysis[6–8] at very low (0.12–0.20 mTorr argon), collisionless pressures that is verified and compared with an RF compensated[9] Langmuir probe. We observe two electron temperature distributions upstream of the double layer and a hotter temperature, a higher energy one downstream of it. For the first time in helicon plasmas to our knowledge, we observe a previously theoretically predicted[10,11] ion hole where the local plasma potential just downstream of the double layer becomes negative. In addition, emissive probe measurements are utilized to measure the plasma potential and its fluctuations. A retarding potential analyzer (RPA) is used to measure the downstream ion beam energy (65 eV) in the lab frame corrected for the local plasma potential and its substantial fraction (77%) of the total ion distribution. In addition, we model the presheath and plasma double layer potential drop via electron and ion currents for the two-temperature upstream and single temperature downstream electron distributions to show that it is comparable to the laboratory measurements and non-Boltzmann in character.

The paper first describes the experimental setup and diagnostic tools, and then the axial variation of the plasma potential and its fluctuations are presented. Then, we present the measurement of a gas temperature at 900 W RF inductive coupling power by spectroscopic means and utilize it to determine by OES as well as RF compensated Langmuir probe measurements of the axial variation of the effective electron temperature. We then examine the spatial variation of the two-Maxwellian electron distributions and their density fraction by OES that are verified by Langmuir probe methods. We then measure the axial variation of the plasma density through the double layer via the millimeter wave interferometer, OES, and Langmuir probe measurements. Next, the accelerated ion beam distribution and its density fraction are measured. We then summarize the conclusions of the research.

II. EXPERIMENTAL SETUP AND DIAGNOSTICS TOOLS

The Madison Helicon eXperiment (MadHeX)[1] (see Fig. 1) consists of an upstream double half-turn helix antenna RF source, a magnetic nozzle, and a downstream magnetic expansion chamber. The Pyrex source chamber is a 120 cm long tube with a 10 cm inner-diameter (ID) dimension. An 18 cm long × 13 cm diameter antenna with an electrically

a)Y.-T. Sung and Y. Li contributed equally to this work.
b)Author to whom correspondence should be addressed. Electronic mail: goesn60812@gmail.com

Reuse of AIP Publishing content is subject to the terms at: https://publishing.aip.org/authors/rights-and-permissions. Downloaded to IP: 128.104.182.119 On: Tue, 11 Oct 2016 19:07:29

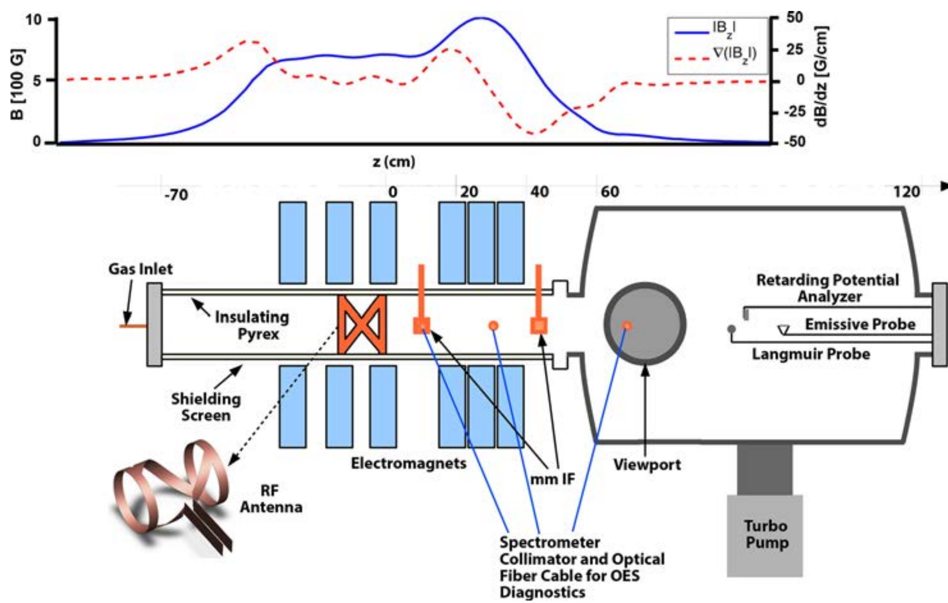

FIG. 1. Madison Helicon eXperiment (MadHeX). The diagnostic tools are indicated within the MadHeX facility. Shown above the system are the spatial variation of the static magnetic field (units in Gauss) and gradient (units in $\frac{\text{Gauss}}{\text{cm}}$). The RF antenna is shown in the lower left corner.

grounded external steel mesh screening (18 cm ID) surrounds the chamber with the downstream edge of the antenna denoting the z = 0 cm position. The expansion chamber is made of stainless steel, which is 70 cm in length with a 45 cm diameter. The Pyrex tube is centered inside the six water-cooled electromagnetic coils. Each is a 7 cm wide with an 18 cm bore. A two-capacitor matching network is used to match the plasma loaded antenna impedance to the RF generator. The matching network is used to couple 900 W to the plasma.

For the current experimental conditions, an axial magnetic field of 340 G in the RF source region is produced by the solenoid magnets. A 900 W of RF power is coupled to the plasma through the antenna at 13.56 MHz via the matching network. Argon gas flows at 2 sccm into the chamber through a copper tube (5 mm ID) attached to an upstream aluminum end plate where the pressure is (0.22 mTorr). This corresponds to a pressure of 0.17 mTorr measured at the junction between the Pyrex tube and the large expansion chamber where the double layer is formed. The electron-neutral momentum mean free path for the $T_e = 4.7$ eV electron cross section[12] at 0.17 mTorr pressure in the double layer region, and the measured $T_g = 500$ K gas temperature is 340 cm. The ion-neutral momentum mean free path for the 65 eV Ar ions[13] at the same pressure and gas temperature is 37 cm. Thus, the electrons and ions are collisionless over the 10 cm long double layer region.

A four-grid (plus a collector) retarding potential analyzer (RPA) (6 mm aperture, 19 mm long, and 27 mm wide) is used to measure the ion energy distribution as a function of source parameters. The collector current is numerically differentiated and then smoothed using a moving average for analysis. The derivative of the collector current determines the energy distribution of the ions falling through the potential drop in front of the RPA and is the ion energy distribution function (IEDF).[14] The RPA data are corrected for the local plasma potential, since the RPA collected ion current is the sum of the ion flow energy and the plasma potential. The ion energy discussed in this paper is the ion flow energy in the laboratory frame that has been corrected for the plasma potential. The plasma potential is obtained via emissive probe measurements.

A swept emissive probe is used to measure the plasma potential. A thoriated tungsten filament, 25 μm in diameter and 6.8 mm long, is spot-welded between two 3 cm long gold-plated nickel wires coated entirely in Sauereisen No. 31 ceramic cement. The probe enters the system through the downstream endplate, and a 90° bend at the end of the probe shaft locates the filament on-axis (r = 0 cm) in the system, oriented perpendicular to the magnetic field.

By sweeping the emissive probe filament bias and measuring the collected current, the plasma potential can be measured using the inflection point method.[15] As the filament current is increased, the inflection point (peak in the first derivative of the collected current with respect to the probe bias voltage) of the I–V trace will approach the plasma potential, when no RF modulation of the plasma potential is present. The plasma potential is calculated in the limit of zero emission by plotting the filament current versus the inflection point voltage. A straight line fit is used to extrapolate to zero emission current, which is interpreted as the plasma potential.

In the presence of plasma potential fluctuations, two or more peaks in the first derivative of the I–V trace may occur, depending on the number of significant harmonics present and the time response of the probe system. The two main peaks are caused by the RF fluctuations at the fundamental. The probe will follow the time averaged plasma potential as the current is varied. The first derivative voltage curve can also be interpreted as a histogram of the values of the plasma potential averaged over many RF cycles, showing the relative amount of time spent at each value. As will be shown further, in our system, there are asymmetric inflection points in the emissive I–V curve, representing the asymmetric RF plasma potential fluctuations, but the time averaged plasma potential can be calculated from the first derivative of the emissive I–V curves using a weighted mean.

The line-averaged electron density (n_e) in the 10 cm diameter Pyrex chamber is determined by our 105 GHz

Reuse of AIP Publishing content is subject to the terms at: https://publishing.aip.org/authors/rights-and-permissions. Downloaded to IP: 128.104.182.119 On: Tue, 11 Oct 2016 19:07:29

Mach-Zehnder millimeter wave interferometer. The phase shift varies linearly with the electron density, given that

$$n_e = \frac{2.07 f \Delta\phi}{d}\ \mathrm{cm}^{-3}, \quad (1)$$

where f is the interferometer frequency in Hz, d is the chamber plasma diameter in cm, and $\Delta\phi$ is the phase shift in degrees.[16,17]

An RF compensated Langmuir probe is used in the MadHeX to determine the electron temperature and density. We fabricated the Langmuir probe based on the design of Sudit and Chen[9] that uses an external floating reference probe, which is several turns of wire around the probe insulator, and connect it through a capacitor to a point between the probe tip and the RF chokes. We compared OES spectral measurements for the electron temperatures with and without the probe present to verify that the probe has a negligible effect on the plasma formed. The fluctuations of the plasma potential are coupled to the measurement probe through the reference windings and a capacitor, which allows the fluctuations to pass and suppresses the time average fluctuation signal. The RF chokes are placed close to the measurement tip to minimize the effect of stray capacitance pickup in a glass tube sealed with a torr-seal to provide a good suppression of the plasma potential fluctuations.

Optical emission spectroscopy (OES) has been widely used as a non-invasive plasma diagnostic, and its ultimate goal is to measure the electron energy distribution of plasmas using optical emission. By comparing the measured spectral line ratios (Argon emission line ratio) with the branching fraction (BF) model, we can obtain the metastable and resonant densities. By comparing emissions from levels populated primarily by high energy electrons (ground state excitation) to emissions from levels populated by low energy electrons (metastable excitation), the effective electron temperature, electron density, and shape of the electron energy distribution can be extracted.[6]

To compare the emission from levels populated with the high-energy electrons to levels with the low energy electrons, the number densities of atoms in the ground state and metastable states must be known. The number density of atoms n_0 in ground state can determined from the ideal gas law $\mathrm{P} = n_0 \mathrm{K} T_g$, where P is the pressure, K is the Boltzmann constant, and T_g is the gas temperature. To determine the gas temperature, a small fraction of nitrogen (10% of the total gas flow rate) is added from the upstream gas port to pure argon, and by comparing the measured nitrogen neutral line emissions (375 nm, 380 nm) with the spectral generated by SPECAIR[18] model calculation, the gas temperature can be obtained.

We assume two standard Maxwellian electron distributions with two different temperatures, one in a lower temperature range (1–5 eV) and one in a higher temperature range (8–20 eV). Then, a list of the number density ratio of the two standard Maxwellian distributions is created. With the combination of the two standard Maxwellian distributions, we will have a non-Maxwellian, two-temperature electron distribution, in which there are three unknown variables, T_{e1}, T_{e2}, and $\frac{n_1}{n_2}$. T_{e1} and T_{e2} are the electron temperatures of the two Maxwellian electron distributions, and $\frac{n_1}{n_2}$ is the density ratio of these two distributions. With the combination of the lists of the three unknowns, the Ar line ratios are calculated according to the OES model and compared with the measured line ratios, and the closest set of calculated line ratio is picked, and the respective T_{e1}, T_{e2}, and $\frac{n_1}{n_2}$ will determine the two-temperature Maxwellian electron distributions of our system, with the density ratio determined from the RF compensated Langmuir probe measurements.

III. PLASMA POTENTIAL MEASUREMENT AT 2 sccm and 900 W

The time average potential profile in MadHeX for the case of 900 W input RF power and 2 sccm flow rate is measured by emissive probes for 20 runs and is shown in Fig. 2. In the upstream region of MadHeX, the plasma potential ranges between 70 V and 80 V (from z = 40 to z = 50 cm). The transition region between the Pyrex tube and the downstream stainless steel expansion chamber with concomitant magnetic field expansion is located from 50 to 60 cm on the z axis. In the interface region, we can see a rapid potential drop from 73 V to −9 V in a range of just 10 cm. Then, from 60 cm to 65 cm, the potential stays negative and forms a negative space potential region. From 65 cm to 80 cm, the plasma potential rises slowly from negative values to about 10 V, forming the downstream boundary of the ion hole structure. We note that, to our knowledge, this is the first time a negative space potential ion hole region has been observed in a helicon plasma source. We observe a maximum potential drop of 85 V in the transition region between the upstream source chamber and the ion hole in the downstream expansion chamber.

IV. RF PLASMA POTENTIAL FLUCTUATION AND SELF-BIAS EFFECT

From Fig. 3, we can see that, in the upstream region ahead of the double layer potential drop, we have a ±25 plasma potential fluctuation of about 40 V peak to peak. At the same time in the downstream expansion chamber, the potential fluctuations are less than ±5%. The lower space potential fluctuation levels in the downstream region might

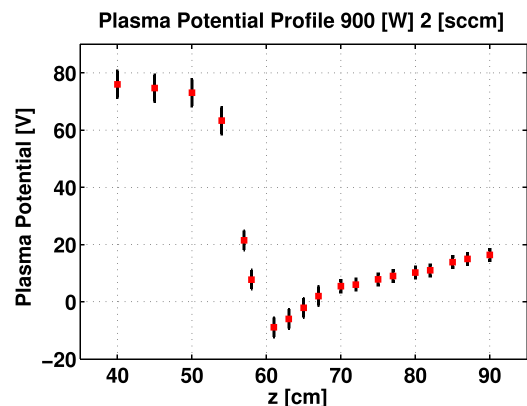

FIG. 2. A time average plasma potential profile for a 900 W and 2 sccm case determined by an emissive probe.

Reuse of AIP Publishing content is subject to the terms at: https://publishing.aip.org/authors/rights-and-permissions. Downloaded to IP: 128.104.182.119 On: Tue, 11 Oct 2016 19:07:29

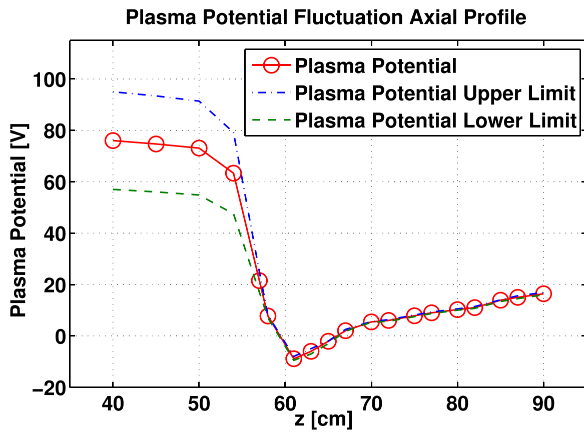

FIG. 3. An axial RF fluctuation evaluation on plasma potential for the case of a 900 W RF input power and a 2 sccm argon flow rate.

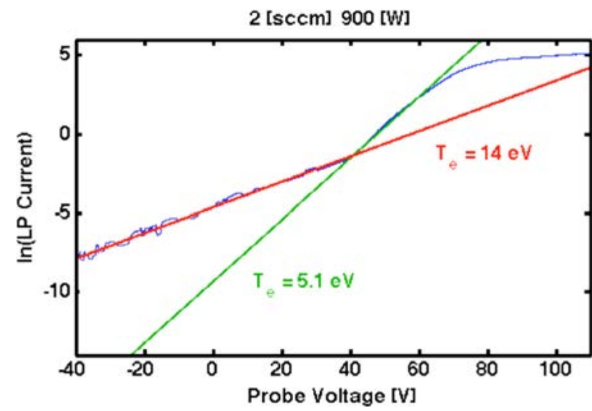

FIG. 4. A RF-compensated Langmuir probe I–V trace (log scale) at z = 40 cm. The electron temperature fitting for bulk and tail electron parts are indicated as green and red lines, respectively.

be caused by the lower electron and ion density existing there and the lower RF power as well as the absence of slower electrons that can support the fluctuations. As we have discussed in Secs. I–III, there are some electrons trapped in the region between the magnetic field nozzle and the double layer potential barrier. Because of the difference in the fluctuation level on the two sides of the double layer structure, when the plasma space potential is lower than its time-averaged value, the potential barrier is also lower for the lower energy trapped electrons. The mobile electrons respond to the lowered potential barrier, while the ions can only respond to the time-averaged potential drop of the double layer. With more electrons passing through the sheath at the interface of the source chamber and expansion chamber, an additional electric field has to be added to the original electric field in the sheath region to accelerate the ions and decelerate the electrons to balance their fluxes in the downstream expansion chamber.

V. TWO-ELECTRON TEMPERATURE MEASUREMENTS

The OES and RF-compensated Langmuir probe diagnostics are used in the Pyrex chamber region upstream of the double layer to examine if a hot, higher energy electron tail distribution exists in the electron energy distribution. From the I–V trace of the RF-compensated Langmuir probe in Fig. 4, we can determine the temperature of the high energy tail electrons by fitting the relatively lower probe biasing voltage at the range from −20 V to 40 V. The tail electron current collected by the Langmuir probe biased at the plasma potential (knee of the I–V trace) can be determined by fitting the I–V curve of the high energy tail electrons and extrapolating it to the plasma potential. For bulk electrons, the electron temperature can be obtained by fitting the bias voltage region from 40 to 60 V. Also, by fitting the semi-log I–V trace of the bulk electrons and extrapolating it to the plasma potential, we can determine the electron current and density contributed by both the bulk and tail electrons. The bulk electron current is obtained by subtracting the tail electron current from the total electron current.

The density ratio of the hot tail electrons to the bulk electrons can be determined by their current ratio obtained from the I–V trace of the RF-compensated Langmuir probe. The theory of Langmuir probe diagnostics indicates that the electron saturation current is given by

$$I_{es} = en_eA\left(\frac{KT_e}{2\pi m}\right)^{1/2}, \tag{2}$$

where n_e is the electron density, A is the probe tip area that is exposed to the plasma, T_e is the electron temperature, and m is the electron mass. The plasma potential can be determined by fitting two straight lines on the I–V trace (on a logarithmic scale) of the RF-compensated Langmuir probe.

The density ratio of the tail and bulk electrons is given by

$$\frac{n_{tail}}{n_{bulk}} = \frac{I_{tail}\sqrt{T_{ebulk}}}{I_{bulk}\sqrt{T_{etail}}}. \tag{3}$$

We also note that the magnetic field can affect the electron saturation current collected by the RF-compensated Langmuir probes. With the magnetic field present, the electrons have to diffuse across the magnetic field lines to be collected by the probe, or the probe will deplete the column defined by the magnetic field line and the intersection with the area of the probe tip. The gyro-radius of the electrons is much less than the probe radius in our case; so, the magnetic field will limit the electron saturation current collection. We are evaluating the density ratio of the bulk and tail electrons. As the same area of the probe tip is used for collecting these two groups, their density ratio will be proportional to their relative electron saturation currents. Also, since the probe tip radius is much larger than the gyro-radii of both tail and bulk electrons, we can neglect the effect of electron gyro-motion collection along the edge of the probe tip.

VI. AXIAL VARIATION OF TWO COMPONENT ELECTRON TEMPERATURES AND DENSITIES

In Fig. 4, we can see that there are two clear slopes in the semi-log I–V trace for the case of a 900 W input RF power and a 2 sccm flow rate of Ar at the position of z = 42 cm, which is just upstream of the double layer. From −10 V to 40 V in the probe bias voltage trace, a fitting slope

Reuse of AIP Publishing content is subject to the terms at: https://publishing.aip.org/authors/rights-and-permissions. Downloaded to IP: 128.104.182.119 On: Tue, 11 Oct 2016 19:07:29

indicates an electron temperature of 14 eV, which is the temperature of tail electrons. From 40 V to 70 V, another slope can be fitted to indicate an electron bulk temperature of 5.1 eV. The density ratio of hot tail electrons to the bulk electrons is determined to be 6%. This value will be utilized for the OES method to analyze the two-temperature Maxwellian electron distributions.

To utilize the OES research developed by Boffard and Wendt[6] to analyze the spectrum for a two-temperature electron distribution function, a distribution function that combines two standard Maxwellian distributions with different temperatures is assumed. The density ratio of the two Maxwellian distributions comes from the line fitting of the RF compensated Langmuir probe. The hot tail electrons account for 6% of the density of the low temperature bulk electrons from the fitting of the I–V trace. The OES results are shown in Fig. 5.

In Fig. 5, we can see that, at the position of 42 cm, just upstream of the double layer structure, the tail electron temperature obtained from OES is 13 eV, while the bulk electron temperature measured is 4.3 eV. The density ratio of the hot tail electrons to the cold bulk electrons associated with the smallest chi square error solution is 6% that also agrees with the Langmuir probe result. With the thermal temperatures of the two standard Maxwellian distributions and their density ratio, we can calculate the effective electron temperature through the following equation:[19]

$$\frac{1}{T_{e,eff}} = \frac{\alpha}{T_{tail}} + \frac{1-\alpha}{T_{bulk}}, \tag{4}$$

where $T_{e,eff}$ is the effective electron temperature and

$$\alpha = \frac{n_{tail}}{n_{tail} + n_{bulk}}. \tag{5}$$

The calculated effective electron temperature at 42 cm is 4.5 eV, which is in close agreement with the effective electron temperature of 4.6 eV measured by OES at 42 cm.

We now compare the two temperatures obtained from the RF compensated Langmuir probe with the bulk and tail electron temperatures from OES at the position of z = 42 cm. The tail electron temperature obtained from the RF compensated Langmuir probe is 14 eV, which is slightly higher than the 13 eV measured by OES. The bulk electron temperature measured by the Langmuir probe is 5.1 eV, which is also slightly higher than the 4.6 eV that is measured by OES. This measurement allows us to determine where the hot electrons in the downstream of the double layer come from. We can see in Figure 5 that there are 6% hot tail electron fraction in the upstream Pyrex source chamber with an electron temperature of 13 eV just upstream of the double layer structure. The density drop over the double layer to about 6% of the upstream value corresponds to the density ratio of untrapped, higher energy tail electrons upstream of the double layer that can transit it. We conclude that the high temperature electrons observed in the expansion chamber downstream of the double layer come from the upstream region ahead of the potential drop. This is also supported by the much lower RF field and fluctuations in the plasma potential (<5%) downstream of the double layer that cannot heat or produce fast electrons.

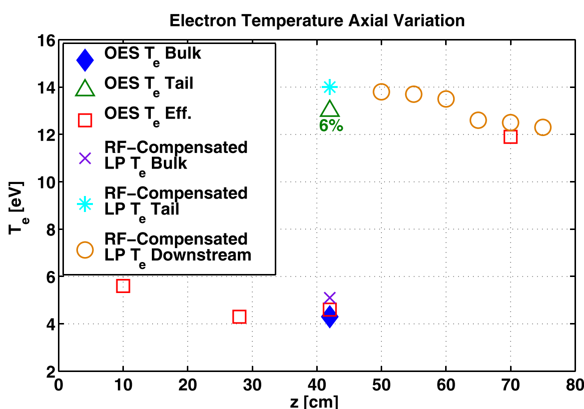

FIG. 5. The two temperature electron temperature measurements from the OES and RF-compensated Langmuir probe.

Many of the hot tail electrons with energies greater than 80 eV can pass through the potential barrier of the double layer structure and transit to the downstream expansion chamber region to balance the accelerated ion current flow. Meanwhile, most of the lower energy, colder bulk electrons are trapped, confined, and reflected by the double layer potential drop, so that the majority of the electrons downstream of the potential drop are primarily hot tail electrons. This is the reason we observe a sudden effective electron temperature rise on the downstream side of the double layer and a significant density drop. Those un-trapped hot tail electrons contribute to the formation of the double layer potential drop that will be discussed later regarding the formation of the double layer and the ion hole structure.

With the aid of the OES and RF-compensated probe measurements, the axial variation of the electron density in MadHeX can also be profiled. For the density measurement by OES, the spectrum is taken and analyzed in the Pyrex chamber upstream of the double layer at z = 10, 28, and 42 cm and in the expansion chamber downstream of the double layer potential drop at z = 70 cm. We also have the electron density measurements at z = 42 cm (upstream of the double layer) to z = 80 cm from the RF-compensated Langmuir probe as well as millimeter wave interferometer data at z = 10 and 42 cm to compare with the OES result.

Since the electron density is measured by fitting the ion saturation current of the Langmuir probe I–V trace, it yields the ion density. If the plasma is quasi-neutral at the position of the measurements of the RF compensated Langmuir probe, we can assume that the measured ion density corresponds to the local electron density. However, in the region of the double layer and ion hole structure, the plasma is not as quasi-neutral, and the electron density measured by the Langmuir probe and shown in Fig. 6 is assumed to be comparable to the ion density.

In Fig. 6, the red squares are the electron densities obtained from OES, and the blue diamonds are the electron densities obtained by the RF compensated Langmuir probe. At the position of z = 10 cm, the electron density obtained by OES is 3.4×10^{11} cm^{-3}. The electron density measured via the interferometry indicates 3.9×10^{11} cm^{-3} and 3.7×10^{11} cm^{-3}

Reuse of AIP Publishing content is subject to the terms at: https://publishing.aip.org/authors/rights-and-permissions. Downloaded to IP: 128.104.182.119 On: Tue, 11 Oct 2016 19:07:29

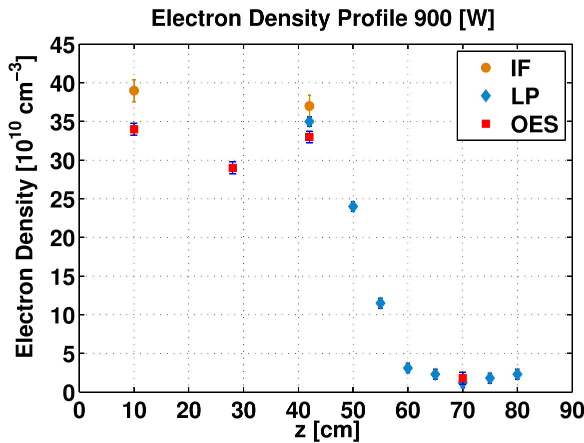

FIG. 6. An electron density profile determined via an interferometry, the OES, and an RF-compensated probe. The red squares are electron densities measured via OES, and the blue diamonds are electron densities measured by an RF-compensated probe. The electron densities obtained from interferometry are indicated by orange circles.

at z = 10 and 42 cm, respectively. At the position of 28 cm in the region of the magnetic nozzle, we have a lower electron density of 2.9×10^{11} cm^{-3}. At the position of 42 cm, just upstream of the double layer potential drop, the observed electron density rises back to 3.3×10^{11} cm^{-3}. In the expansion chamber downstream of the double layer at the position z = 70 cm, the electron density drops to 1.8×10^{10} cm^{-3}, which is 18 times lower (or 6%) compared to the electron density measured just ahead of the double layer.

We can see that the electron density at 28 cm is somewhat lower than the upstream electron density at 12 cm and the downstream electron density at 42 cm. This region is where the magnetic nozzle is located with its peak magnetic field. Thus, the electrons with relatively lower energies parallel to the constant magnetic field will be reflected by the magnetic mirror, and this is a possible explanation as to why we have a somewhat lower electron density in the magnetic nozzle region at z = 28 cm than that at z = 10 cm. Between the magnetic field nozzle and double layer potential drop, some of the lower energy electrons will be trapped, and some of the electrons downstream of the double layer that are moving upstream will be accelerated through the double layer. This is an explanation as to why we have the electron density rising from z = 28 cm to 42 cm just ahead of the double layer.

From the electron densities determined by the RF-compensated probe measurements, we can see that the electron density at 42 cm is 3.5×10^{11} cm^{-3}, which agrees well with that determined by OES (3.3×10^{11} cm^{-3}). From z = 50 cm to 65 cm, the double layer potential drop and ion hole potential dip region, the quasi-neutrality is not as well satisfied, and it is actually the ion density we measure. We see that the ion density drops from 3.5×10^{11} cm^{-3} to 2.3×10^{10} cm^{-3} from z = 50 cm to 65 cm, which is due to both the expansion of the magnetic field lines and the acceleration of ions just downstream of the double layer. We see that the ion density has a sharp drop from 42 cm to 60 cm, which agrees with the potential drop region of the double layer structure. Then, the density reaches its minimum value of 1.2×10^{10} cm^{-3} at z = 70 cm, obtained from Langmuir probe measurements and is close to the electron density measured via OES of 1.8×10^{10} cm^{-3}. Further downstream from z = 70 cm, the ion density measured by the Langmuir probe rises again slowly to 2.3×10^{10} cm^{-3} at the position z = 80 cm, which is caused by the ion deceleration resulting from the plasma space potential rise downstream from the ion hole region.

VII. RPA ION BEAM AND DENSITY FRACTION

The 65 eV ion-neutral charge exchange mean free path in the expansion chamber in the 900 W, 2 sccm flow rate case is comparable to the length of the expansion chamber in MadHeX. Thus, we should be able to observe an ion beam flowing in the downstream expansion chamber region that is accelerated by the electrical field in the double layer region. The ion beam is detected by a grounded 4-grid retarding potential analyzer (RPA) with the ion beam energy and plasma potential profile shown in Fig. 7.

In Fig. 7, the space potential determined from the swept emissive probe is indicated by red markers. The blue markers show the ion beam energy determined from the RPA measurements. The ion beam energy rises rapidly from z = 50 to 60 cm and reaches 80 eV, which is the maximum value, at z = 60 cm. This is the region where we have the deep potential drop of the double layer structure and the lowest space potential in the ion hole region. The ion beam energy then decreases slowly from 80 eV to 60 eV from z = 60 to z = 75 cm and then varies slowly near 60 eV beyond z = 75 cm. The decrease of the ion beam energy in this region is caused by the rising plasma potential on the downstream side of the ion hole structure, which results in some deceleration of the beam ions.

In Fig. 8, the ion energy distribution function profiled at z = 85 cm for 900 W and 2 sccm is represented as the blue line. The lower discriminator voltage peak at around 15 V near the plasma potential indicates a bulk ion energy

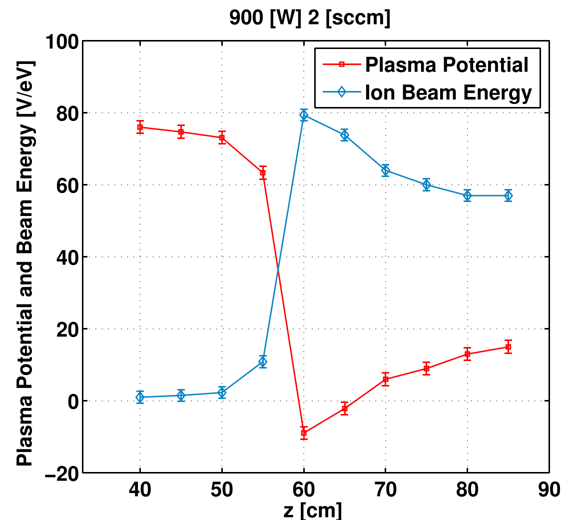

FIG. 7. An ion beam profile determined through retarding potential analyzer and plasma potential profile from the upstream to the downstream region. The blue diamonds represent the ion beam energy, and the red squares represent the plasma potential.

Reuse of AIP Publishing content is subject to the terms at: https://publishing.aip.org/authors/rights-and-permissions. Downloaded to IP: 128.104.182.119 On: Tue, 11 Oct 2016 19:07:29

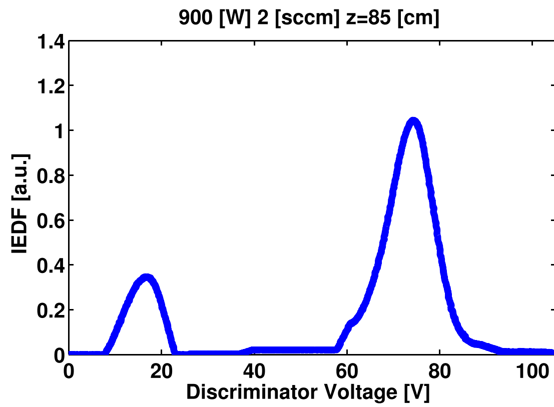

FIG. 8. An ion energy distribution function determined through the four-gird retarding potential at z = 85 cm for a 900 W and 2 sccm case.

detected by the RPA, while the larger, higher discriminator voltage peak at around 75 V represents the beam energy. We also estimate via Gaussian fitting that a lower bound for the beam fraction at this position is ∼77% of the total ion density by using the formula stated as follows:

$$\frac{n_{beam}}{n_{bulk}+n_{beam}} = \frac{\dfrac{I_{beam}}{v_{beam}}}{\dfrac{I_{bulk}}{c_s}+\dfrac{I_{beam}}{v_{beam}}}. \tag{6}$$

This is a lower bound for the beam fraction since ions with transverse energies greater than 0.1 eV will be lost and not collected by the small diameter (0.8 cm) RPA.

VIII. SCAN OF FLOW RATE PRESSURE VARIATION ON THE ION HOLE

A flow rate scan from 1.5 sccm to 2.0 sccm and 2.5 sccm at a net coupled power of 900 W was carried out to observe the effects of neutral pressure and the high energy tail electrons effects on the double layer structure. In the case of 1.5 sccm, the gas pressure near the double layer and ion hole region is 0.15 mTorr. In the case of 2.5 sccm flow rate, the gas pressure in downstream expansion chamber is 0.20 mTorr. For the same input power level, a higher flow rate should lead to a higher electron density and a lower electron temperature, along with a lower high energy tail electron density relative to the ion density, and thus a lower plasma space potential drop across the double layer structure. The space potential profiles are as shown in Fig. 9.

We note that, at the higher flow rate and neutral pressure at 2.5 sccm, the ion hole is not present with the plasma potential remaining positive throughout the double layer region and the total potential drop over the double layer is reduced. For the lowest flow rate of 1.5 sccm, the ion hole region is maximized, and the net potential drop from the upstream to downstream region is substantially increased.

In Figs. 9 and 10, we can see that the plasma potential drop increases when the input gas flow rate decreases. In the upstream region, the plasma potential drops from 86 V at the flow rate of 2.5 sccm to 71 V at 1.5 sccm. In the expansion chamber, downstream side of the double layer structure, the lowest space potential also drops with lower flow rates, from 8 V at the flow rate of 2.5 sccm to −20 V at 1.5 sccm. As a result, we have a larger potential drop across the double layer structure with lower flow rates, which is 75 V at 2.5 sccm and rises to 90 V at 1.5 sccm. The ion beam energy profile of the gas flow rate scan is as shown as in Fig. 10. The highest ion beam energy is obtained for the case of 1.5 sccm, while a lower ion beam energy is observed at 2.5 sccm flow rates. This agrees with the magnitude of plasma potential drop in the flow rate scan analysis. Although all the three cases have a low Ar pressure and the mean (particle-neutral) free path for electrons and ions is 50 cm for ions and 200 cm for electrons, the double layer and potential drop vary significantly with the neutral pressure.

The electron density profiles determined by OES for the three flow rate cases are shown in Fig. 11. We observe that, with the decreasing gas input flow rates, the electron densities measured near the antenna downstream edge (at z = 12 cm), on the double layer upstream side, and on the downstream of the double layer also decrease. At the position of 12 cm, there is a relatively large density decrease from $4.5 \times 10^{11}\ \mathrm{cm}^{-3}$ at a flow rate of 2.5 sccm to $2.3 \times 10^{11}\ \mathrm{cm}^{-3}$ at 1.5 sccm.

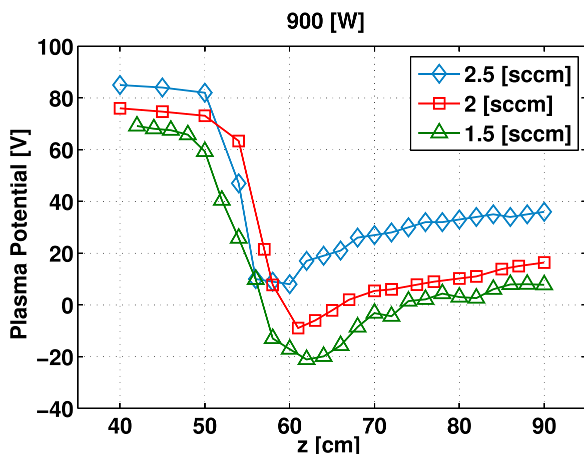

FIG. 9. The plasma potential profiles for an argon gas input flow rate scan. The red line is the standard 2 sccm flow rate, the blue line represents the 2.5 sccm flow rate case, and the green line is the 1.5 sccm flow rate case.

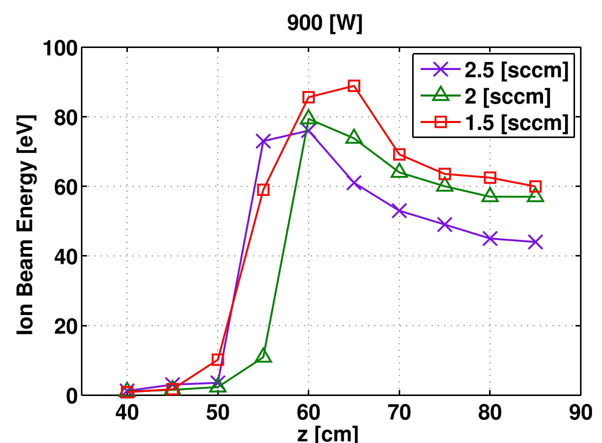

FIG. 10. An ion beam energy profile for different flow rates. The green line is the standard 2 sccm flow rate, the purple line represents the 2.5 sccm flow rate case, and the red line is the 1.5 sccm flow rate case.

Reuse of AIP Publishing content is subject to the terms at: https://publishing.aip.org/authors/rights-and-permissions. Downloaded to IP: 128.104.182.119 On: Tue, 11 Oct 2016 19:07:29

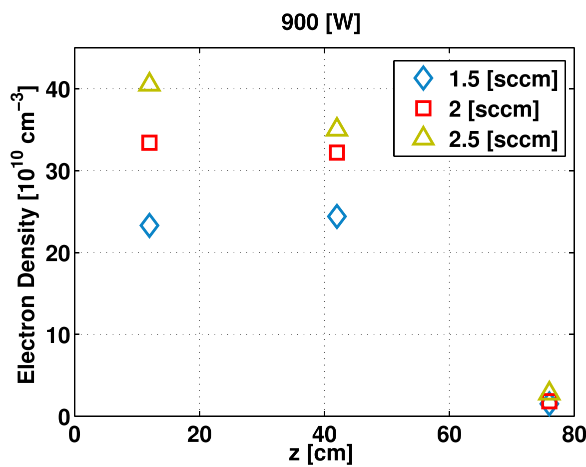

FIG. 11. An electron density profile determined through the OES for the flow rate scan.

However, at the position of 42 cm, between the magnetic field nozzle and the double layer potential drop, the electron density decrease is smaller, from 3.5×10^{11} cm^{-3} at 2.5 sccm to 2.4×10^{11} cm^{-3} at 1.5 sccm. This could arise from the electron trapping mechanisms near the upstream magnetic mirror and the downstream double layer potential barrier. The electrons can be trapped in this region and heated for a longer time than electrons in other regions. Also, collisionless Landau damping[20] might also provide heating mechanisms in this region, which can contribute to enhance the formation of the hotter, high energy tail electrons. Also, in the case of the 1.5 sccm flow rate the electron density determined via OES is slightly higher at $z = 42$ cm than the electron density at the position of $z = 12$ cm. This supports the possibility of trapping and heating of the electrons in the region between the magnetic nozzle and double layer potential barrier.

Utilizing OES and the density ratio of the high temperature to low temperature determined by the RF compensated Langmuir probe measurements, we can obtain the fast and bulk electron temperatures. The ratio of the tail electron density to the bulk electron density as noted in Eq. (3) can also be obtained for the following cases. For the case of 1.5 sccm at 42 cm, the bulk electron measured temperature is 4.7 eV, and the electron temperature of the tail electrons is 15 eV. The tail electron density accounts for about 9% of the density of bulk electrons. At the position of 70 cm, the effective electron temperature measured is 13 eV. The electron temperatures of both the bulk and tail electrons in the case of 1.5 sccm flow rate are higher than those in the case of 2 sccm. Although, in the case of 1.5 sccm, the total electron density decreases, the percentage and temperature of the electrons that can pass through the double layer barrier increase.

The relative electron density compared to the ion density just downstream of the double layer structure increases at lower pressures, which explains why we have a deeper potential dip and ion hole for the 1.5 sccm flow rate. The same analysis also applies to the case of a 2.5 sccm flow rate. For the 2.5 sccm flow rates, at the position $z = 42$ cm, the bulk electron temperature measured is 4.0 eV, and the tail electron temperature measured is 11 eV, which is just 4% of the bulk electron density. These results illustrate the sensitivity of the neutral pressure in producing a hot electron component and the significant effect of the hot electrons in producing the ion hole.

IX. SUMMARY AND CONCLUSIONS

We have observed a potential drop of 80 V for an ion acceleration with a double layer-like structure in the Madhex Helicon Experiment. The helicon plasma source with a magnetic nozzle operated in a high power, low pressure condition produces a two-temperature Maxwellian electron distribution with a hotter, high energy electron tail, which increases the electron flux that can pass through the potential barrier and, thus, enhances the potential drop across the double layer structure. We have observed $\pm 25\%$ RF plasma potential fluctuations in the upstream region and smaller 5% fluctuations downstream of the double layer-like structure. The upstream RF fluctuations increase the number of electrons that can pass through the double layer during the period when the potential barrier is lower, thus enhancing the potential drop through the self-bias effect. To our knowledge, this is the first time that a theoretically predicted ion hole with a negative plasma potential is formed in a helicon plasma source. The ion hole region has an excess electron density locally and acts as a negatively charged layer, forming the other side of the double layer structure with the upstream the ion sheath region. The lower ion density and higher electron density in this region is caused by the fact that the ions are accelerated to a high speed when the reach the ion hole region and the electrons are decelerated in the same region.

An ion beam is accelerated through the potential gradient in the double layer region and flows downstream of the expansion chamber with an energy 65 eV that is 77% of the ion distribution is observed by a retarding potential analyzer. A possible electron trapping is observed in the region between the magnetic nozzle and the double layer potential drop. This trapping effect contributes to the heating of the electrons and the formation of the hot, high energy electron tail.

ACKNOWLEDGMENTS

We thank Dr. Boffard and Professor Wendt for their helpful discussions on the OES diagnostics they have developed. This research was supported in part by the University of Wisconsin.

[1]Y.-T. Sung, Y. Li, and J. E. Scharer, Phys. Plasmas 22, 034503 (2015).
[2]M. Wiebold, Y.-T. Sung, and J. E. Scharer, Phys. Plasmas 19, 053503 (2012).
[3]M. Wiebold, Y.-T. Sung, and J. E. Scharer, Phys. Plasmas 18, 063501 (2011).
[4]K. Takahashi, C. Charles, R. W. Boswell, T. Kanedo, and Hatakeyama, Phys. Plasmas 14, 114503 (2007).
[5]X. Sun, A. Keesee, C. Biloiu, E. Scime, A. Meige, C. Charles, and R. Boswell, Phys. Rev. Lett. 95, 025004 (2005).
[6]J. B. Boffard, R. O. Jung, C. C. Lin, and A. E. Wendt, Plasma Sources Sci. Technol. 18, 035017 (2009).
[7]J. B. Boffard, R. O. Jung, C. C. Lin, and A. E. Wendt, Plasma Sources Sci. Technol. 19, 065001 (2010).
[8]S. Wang, A. E. Wendt, J. B. Boffard, C. C. Lin, S. Radovanov, and H. Persing, J. Vac. Sci. Technol. 31, 021303 (2013).

Reuse of AIP Publishing content is subject to the terms at: https://publishing.aip.org/authors/rights-and-permissions. Downloaded to IP: 128.104.182.119 On: Tue, 11 Oct 2016 19:07:29

[9]I. D. Sudit and F. F. Chen, Plasma Sources Sci. Technol. **3**, 162–168 (1994).
[10]H. Schamel, Phys. Rep. **140**(3), 161–191 (1986).
[11]H. Schamel and S. Bujarbarua, Phys. Fluids **23**, 2498 (1980).
[12]A. Zecca, G. P. Karwasz, and R. Brusa, Riv. Nuovo Cimento **9**(3), 1146 (1996).
[13]A. V. Phelps, J. Phys. Chem. Ref. Data **20**, 557 (1991).
[14]P. Chabert and N. Braithewaite, *Physics of Radio-Frequency Plasmas* (Cambridge University Press, 2011).
[15]J. P. Sheehan and N. Hershkowitz, Plasma Sources Sci. Technol. **20**, 063001 (2011).
[16]C. M. Denning, Ph.D. thesis, University of Wisconsin at Madison, 2008.
[17]C. M. Denning, M. Wiebold, and J. Scharer, Phys. Plasmas **15**, 072115 (2008).
[18]C. O. Laux, Ph.D. thesis, Stanford University, 1993.
[19]J. P. Sheehan and N. Hershkowitz, J. Vac. Sci. Technol. **30**, 031302 (2012).
[20]D. G. Swanson, *Plasma Waves*, 2nd ed. (Institute of Physics Publishing, Bristol and Philadelphia, 2003).

Reuse of AIP Publishing content is subject to the terms at: https://publishing.aip.org/authors/rights-and-permissions. Downloaded to IP: 128.104.182.119 On: Tue, 11 Oct 2016 19:07:29